

# System Performance Insights into Design of RIS-assisted Smart Radio Environments for 6G

Mehdi Toumi, Adnan Aijaz

Bristol Research and Innovation Laboratory, Toshiba Europe Ltd., Bristol, United Kingdom

mehdi.toumi@toshiba-bril.com, adnan.aijaz@toshiba-bril.com

**Abstract**—In state-of-the-art wireless networks, the radio environment is beyond the control of the operators which leads to several issues. For example, signal attenuation limits radio connectivity, multi-path propagation results in fading phenomena and reflections/refractions from large objects are the main sources of uncontrollable interference. To overcome these issues, a new technology referred to as reconfigurable intelligent surfaces (RISs) has been brought to light. RISs, whose interactions with the electromagnetic waves are reconfigurable, are at the heart of the *smart radio environments* for beyond 5G (or 6G) wireless systems. Research on design of smart radio environments is still in infancy. To this end, this paper provides performance insights for design of RIS-assisted smart radio environments. By extending a recent system-level simulator and through extensive simulations, it investigates the impact of positioning/placement of RISs, the number of reflecting elements and the tilt/rotation of RISs in both single and multi-RIS environments. Results reveal that these aspects are crucial to achieving capacity and reliability enhancements in smart radio environments.

**Index Terms**—6G, beyond 5G, capacity, metasurface, RIS, reliability, smart radio environments.

## I. INTRODUCTION

Current technologies assisting the Physical (PHY) layer in wireless communications consist mainly of multiple-input multiple-output (MIMO) / massive MIMO beamforming, relaying and backscattering. These technologies are used for the purpose of tackling the limitations of scatters from large scale buildings and small-sized objects. The reason behind this vulnerability is due to the use of sub-6 GHz frequency bands which will soon not be able to meet the growing data rate requirements and will necessitate migration to mmWave and higher frequencies. Furthermore, legacy wireless communications lacks control over the wave propagation environment. The new wireless environment is envisioned within an architectural platform where the propagation of radio waves is controllable and programmable. This concept goes by *smart radio environment* (SRE) [1] and consists of intentionally and deterministically controlling the signal propagation in the radio environment. The key technology underpinning SREs is reconfigurable intelligent surfaces (RISs) which have also been called metasurfaces, large intelligent surfaces (LISs) and intelligent reflective surfaces (IRSs). RISs consist of many anomalous controllable reflecting electromagnetic surfaces capable of changing the phase of the landing waves. It is a nearly passive new technology that, conversely to currently employed technologies, does not require signal processing nor signal amplification processes. The simple act of reflecting the

waves from its surface spares the signal from additional noise. Moreover, it operates in full band spectrum and is easy and cheap to deploy.

## A. Related Work

Ongoing research activities are investigating various aspects of RIS-assisted communication. Kudathanthirige *et al.* [2] conducted an analysis of achievable data rate and average symbol error probability for RIS-assisted communication between a Tx and a Rx. The accuracy of closed-form expressions has been shown to improve as the number of reflecting elements on the RIS increases. Hu and Rusek [3] investigated deployment of RISs in three-dimensional (3D) as spherical surfaces which provide various advantages over their planar counterparts such as higher coverage and ease of deployment and placement. Ntontin *et al.* [4] and Björnson *et al.* [5] conducted thorough comparison of RIS and relaying technologies. Both studies conclude that RIS-assisted communication achieves better performance than relaying-assisted communication for large number of antenna elements. Moreover, it is easier to manipulate impinging signals at an electromagnetic level than in the digital domain as in the case of decode and forward relays. Boulogeorgos and Alexiou [6] conducted a performance comparison of RISs and amplify-and-forward (AF) relaying systems. The authors show that RIS-assisted wireless systems outperform AF-relaying ones in terms of outage probability and ergodic capacity. Comparative studies of RIS and massive MIMO technologies have been the focus of some recent studies. The work of Dardari [7] shows that RIS offers more degrees-of-freedom (DoF) which is particularly beneficial for mmWave communication. Björnson and Sanguinetti [8] compared power scaling laws and near-field behavior of the two technologies. The authors prove that an RIS-assisted setup cannot achieve a better signal-to-noise ratio (SNR) than an equal-sized massive MIMO setup. Some recent studies (e.g., [9] and [10]) have also explored the use of RIS as a tool for positioning/localization.

## B. Contributions and Outline

The objective of this paper is to provide system performance insights for design of RIS-assisted SREs. Existing studies evaluating the performance of RIS-assisted communication are mostly focused on theoretical frameworks and independently treat the impact of different parameters for a SRE. We adopt a simulation-driven approach and conduct a holistic evaluation

of capacity and reliability aspects by simultaneously considering different parameters. We also evaluate system performance under single and multiple RIS-assisted SREs. To this end, our key contributions are summarized as follows.

- The positioning of RISs is a crucial factor for RIS-assisted SREs. We prove that its closeness to the endpoints or its placement above the transmitter level boosts system performance. More importantly, it improves drastically in a multiple RIS environment.
- A key RIS application involves sensing and localization. In this paper, we explore the tilt and rotation aspects of RISs and investigate the system performance. Our simulations demonstrate performance enhancements when the RIS focuses the reflected beam toward the receivers.
- The number of reflecting elements on a single RIS is another determinant factor in the system performance. We prove that the capacity and reliability increase considerably for larger number of reflecting elements. The channel shows a very slight improvement for small number of elements. However, multi-RIS configuration curtails performance issue of reduced number of reflecting elements. This highlights a trade-off in the design aspect of RISs.

The rest of the paper is structured as follows. Section II introduces the adopted simulator and our key enhancements. In Section III we provide a system model for RIS-assisted SRE. Section IV covers our performance evaluation of RIS-assisted SREs. Key insights, concluding remarks, and future work directions are provided in Section V.

## II. SIMRIS SIMULATOR AND ENHANCEMENTS

Our performance evaluation is based on a state-of-the-art simulator for RIS-assisted communication, i.e., SimRIS [11], which is an open-source channel simulator. It models RIS-empowered radio environments over two operating frequencies (28 GHz – 73 GHz) where for a given number of reflecting elements  $N$ , the user positions the  $N$ -element RIS in ‘xz’ or ‘yz’ plane in an indoor or outdoor environment. The channel responses  $h$ ,  $g$ ,  $h_{SISO}$  for the transmitter-to-RIS (Tx-RIS), RIS-to-receiver (RIS-Rx), transmitter-to-receiver (Tx-Rx) links respectively are given by the simulator. Nevertheless, in this paper, we compute our own RIS matrix (final result in (9)) that represents RIS contribution in the radio environment. On top of that, we re-arranged the channel links to investigate the possibility to tilt and rotate the intelligent surface as can be seen in (12). We also aimed at exploring the influence of number of elements ( $N$ ) dependently on number of RISs ( $M$ ) deployed in a multi-RIS assisted environment [12]. On that front, we addressed a trade-off between these two parameters. This could be a significant steppingstone for the physical conception of RISs. Another element of simulation is the multi-user scenario where we allocate certain reflecting elements from a single surface to each user.

## III. SYSTEM MODEL

Our system model for the RIS-assisted smart radio environment in Fig. 1 consists of a Tx, a Rx and an RIS composed of

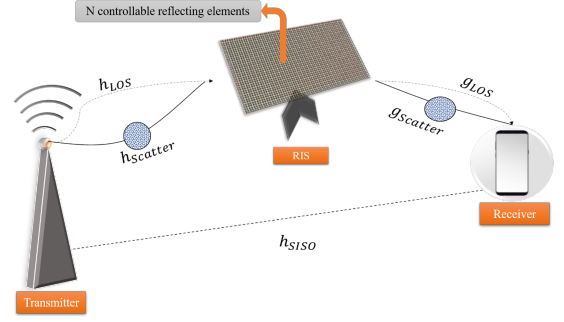


Fig. 1: System model for RIS-assisted radio environment.

$N$  controllable reflecting elements. If we consider  $h$  as the Tx-RIS channel response and  $g$  as the RIS-Rx channel response, we have  $h = h_{Scatterer} + h_{LOS}$  and  $g = g_{Scatterer} + g_{LOS}$  where  $h_{LOS}$  and  $g_{LOS}$  are line of sight (LOS) links.  $h_{Scatterer}$  and  $g_{Scatterer}$  are links due to scatterers. It has been discussed in [11] that the received discrete time baseband signal can be written as:

$$y = (g^T \times \phi \times h) \cdot x \quad (1)$$

where  $h \in \mathbb{C}^{N \times 1}$  and  $g \in \mathbb{C}^{N \times 1}$  ( $N \times 1$  complex matrices) and  $\phi$  is the matrix of RIS elements' response. However, in case of the presence of a direct link between Tx and Rx, it can be included in the expression above as follows [11]:

$$y = (g^T \times \phi \times h + h_{T_x-R_x}) \cdot x \quad (2)$$

In the same way the direct link between  $T_x$  and  $R_x$  is incorporated into the model, originating from the equation 2, we are suggesting that the received signal in case of adding a second RIS can be expressed as:

$$y = (g_1^T \times \phi_1 \times h_1 + g_2^T \times \phi_2 \times h_2 + h_{T_x-R_x}) \cdot x \quad (3)$$

In a more general way, for an  $M$ -RIS assisted system, the expression of the received signal can be written as:

$$y = \left( \sum_M g_M^T \times \phi_M \times h_M + h_{T_x-R_x} \right) \cdot x \quad (4)$$

The following content in this subsection is a summary of RIS channel response introduced in [11]. We consider  $C$  the number of clusters and for each cluster  $c$  there are  $S_c$  scatterer. The channel coefficients ( $h$ ) can be calculated as follows:

$$h = \gamma \sum_{c=1}^C \sum_{s=1}^{S_c} \beta_{c,s} \sqrt{G_e(\theta_{c,s}^{RIS}) L_{c,s}^{RIS}} a(\phi_{c,s}^{RIS}, \theta_{c,s}^{RIS}) + h_{LOS} \quad (5)$$

where the normalization factor is  $\gamma = \sqrt{\frac{1}{\sum_c S_c}}$ ,  $\beta_{c,s}$  is the path gain following a complex normal distribution  $\mathcal{CN}(0, 1)$  and  $L_{c,s}^{RIS}$  is the path attenuation of the propagation in the  $(c, s)$  scatterer path.  $G_e(\theta_{c,s}^{RIS})$  represents the RIS gain for the  $(c, s)$  th scatterer and the RIS array response vectors is  $a(\phi_{c,s}^{RIS}, \theta_{c,s}^{RIS}) \in \mathbb{C}^{N \times 1}$  which is a function of the Azimuth angle (RIS arrival)  $\phi_{c,s}^{RIS}$  and the Elevation angle (RIS arrival)  $\theta_{c,s}^{RIS}$ . On the other hand,  $h_{LOS}$  can be calculated as:

TABLE I: Key Simulation Parameters

Parameter	Value
No. of elements ( $N$ )	Variable
Pathloss exponent ( $n$ )	3.19 (non-LOS), 1.73 (LOS)
Operating frequency ( $f$ )	73 GHz
Pathloss parameter ( $b$ )	0.06 (non-LOS), 0 (LOS)
Variance ( $\sigma$ )	8.29 dB (non-LOS), 3.02 dB (LOS)

$$h_{LOS} = I_{h(d_{T-RIS})} \sqrt{G_e(\theta_{LOS}^{RIS}) L_{LOS}^{Tx-RIS}} e^{j\eta} a(\phi_{LOS}^{RIS}, \theta_{LOS}^{RIS}) \quad (6)$$

where  $I_{h(d_{T-RIS})} \in \{0, 1\} \sim B(1, p)$  is a random variable that determines whether a LOS link exists for Tx-RIS path separated with  $d_{T-RIS}$ .  $G_e(\theta_{LOS}^{RIS})$  is the RIS gain from the direction of LOS. As for  $L_{LOS}^{Tx-RIS}$ , it represents the attenuation of the LOS link in Tx-RIS path.  $\eta \sim U[0, 2\pi]$  is a random phase term and  $a(\phi_{LOS}^{RIS}, \theta_{LOS}^{RIS})$  is the RIS array response vector.

Second link in the RIS-assited communication path is  $g$ , which characterizes the RIS to Rx channel coefficients.  $g$  is evaluated through (7) below.

$$g = \sqrt{G_e(\theta_{Rx}^{RIS}) L_{LOS}^{RIS-R}} e^{j\eta} a(\phi_{Rx}^{RIS}, \theta_{Rx}^{RIS}) \quad (7)$$

where  $a(\phi_{Rx}^{RIS}, \theta_{Rx}^{RIS})$  is the RIS array response vector (Rx) and  $G_e(\theta_{Rx}^{RIS})$  is the gain of RIS element in the direction of Rx. The attenuation of LOS RIS-Rx channel is denoted by  $L_{LOS}^{RIS-R}$  and  $\eta \sim U[0, 2\pi]$  represents a random phase term.

Vis-à-vis the channel between Tx and Rx, it is represented in  $h_{SISO}$  and computed through the following equation:

$$h_{SISO} = \gamma \sum_{1 < c < C} \sum_{1 < s < S_c} \beta_{c,s} e^{j\eta_e} \sqrt{L_{c,s}^{SISO}} + h_{LOS} \quad (8)$$

First, we assume the use of single-input single-output (SISO) endpoints. Then we make the assumption that the RIS and Rx share the same clusters in Tx-RIS and Tx-Rx links, which results in the same  $\gamma$ ,  $C$ ,  $S_c$ ,  $\beta_{c,s}$  and finally the LOS component  $h_{LOS}$ . In (8),  $L_{c,s}^{SISO}$  represents the attenuation in path of Tx-Scatterer-Rx and  $\eta_e$  is the phase excess due to the difference between the distance separating Tx-RIS and Tx-Rx through the same scatters. If we consider the scatterer ( $c,s$ ) and its distances from RIS and from the Rx respectively denoted by  $b_{c,s}$  and  $\hat{b}_{c,s}$ , we find:  $\eta_e = k(b_{c,s} - \hat{b}_{c,s})$ .

#### A. Conception of $\phi_m$ where $1 < m < M$

In (2), SimRIS provides  $g$  and  $h$  and  $h_{T_x-R_x}$ . However, the matrix  $\phi_N$ , a key matrix that optimizes the communication by maximising the SNR and is conceptualized in this paper as follows: if we assume a full knowledge of  $g$  and  $h$  and  $h_{T_x-R_x}$ , we determine the phase that maximises the received signal as to be the opposite of the sum of the phases of  $g$  and  $h$  added to  $h_{T_x-R_x}$  phase.  $\phi_N$  is expressed below:

$$\phi_m = \text{diag}(\alpha e^{-i(\phi_{g1,m} + \phi_{h1,m} + \phi_{h_{T_x-R_x}})} \dots \alpha e^{-i(\phi_{gn,m} + \phi_{hn,m} + \phi_{h_{T_x-R_x}})}) \quad (9)$$

where  $m$  is the  $m$ th intelligent surface composed of  $N$  number of elements. Considering  $k$  where  $1 < k < N$ , we have  $\phi_{gk,m}$  is the phase of the link between the Tx and the  $k$ th element of the RIS,  $\phi_{hk,m}$  is the phase of the link between the

Rx and the  $k$ th element of the RIS and  $\phi_{h_{T_x-R_x}}$  is the phase of the direct link between the Tx and the Rx.

#### B. Array Response Vectors and Complex Path Attenuation

The array response vectors consist of  $a(\phi_{c,s}^{RIS}, \theta_{c,s}^{RIS})$ ,  $a(\phi_{LOS}^{RIS}, \theta_{LOS}^{RIS})$ ,  $a(\phi_{Rx}^{RIS}, \theta_{Rx}^{RIS})$  evaluated in a similar manner for the different parameters and calculated as follows:

$$a(\phi_{c,s}^{RIS}, \theta_{c,s}^{RIS}) = [1 \dots e^{jkd(x \sin \theta_{c,s}^{RIS} + z \sin \phi_{c,s}^{RIS} \cos \theta_{c,s}^{RIS})} \dots e^{jkd((\sqrt{N}-1) \sin \theta_{c,s}^{RIS} + (\sqrt{N}-1) \sin \phi_{c,s}^{RIS} \cos \theta_{c,s}^{RIS})}]^T \quad (10)$$

As for the complex path attenuations  $L_{LOS}^{T-RIS}$ ,  $L_{LOS}^{RIS-R}$ ,  $L_{C,S}^{SISO}$ ,  $L_{C,S}^{RIS}$ , they are evaluated in the same way using (11) considering different distances for the corresponding path ( $d_{T_x-RIS}$ ,  $d_{RIS-R_x}$ ,  $d_{cs-SISO}$ ,  $d_{cs-RIS}$ ) where  $d_{T_x-RIS}$  is distance between Tx and RIS and  $d_{RIS-R_x}$  represents the distance between RIS and Rx while  $d_{cs,SISO}$  is the total distance Tx-Scatterer-Rx and  $d_{cs-RIS}$  is total distance Tx-Scatterer-RIS.

$$L_{c,s}^{RIS} = -20 \log_{10} \left( \frac{4\pi}{\lambda} \right) - 10n \left( 1 + b \left( \frac{f - f_0}{f_0} \right) \right) \log_{10}(d_{c,s}) - X \quad (11)$$

In (11),  $X_\sigma \sim N(0, \sigma^2)$  represents a shadow factor. As for the operating frequency  $f$ , RIS operates in full band. This property of RIS is one of its biggest advantages since mmWave is the key ensuring the requirements of increasing data rates. Details of the pathloss parameters  $n$ ,  $\sigma$ ,  $f_0$  and  $b$  can be found in [13].

#### C. Tilt of the Intelligent Surface

In the tilt simulations, the coordinates of the RIS reflecting elements are:  $(x, 0, z)$  where  $x$  and  $z \in 1, \dots, \sqrt{N}-1$ . The tilt simulation of an angle  $R$  is applied by multiplying RIS reflecting elements' coordinates by the rotational matrix. Those interfere in the RIS array response vectors  $a(\phi_{c,s}^{RIS}, \theta_{c,s}^{RIS})$ ,  $a(\phi_{LOS}^{RIS}, \theta_{LOS}^{RIS})$  and  $a(\phi_{Rx}^{RIS}, \theta_{Rx}^{RIS})$  as in (12).

#### IV. PERFORMANCE OF RIS-ASSISTED ENVIRONMENTS

In this section we conduct an evaluation of RIS-assisted radio environments based on our enhanced version of SimRIS simulator. The key simulation parameters are highlighted in TABLE I.

$$a(\phi_{c,s}^{RI}, \theta_{c,s}^{RIS}) = [1 \dots e^{jkd(x \sin \theta_{c,s}^{RIS} + (z \cos R) \sin \phi_{c,s}^{RIS} \cos \theta_{c,s}^{RIS} - (z \sin R) \cos \phi_{c,s}^{RIS} \cos \theta_{c,s}^{RIS})} \dots e^{jkd((\sqrt{N}-1) \sin \theta_{c,s}^{RIS} + ((\sqrt{N}-1) \cos R) \sin \phi_{c,s}^{RIS} \cos \theta_{c,s}^{RIS} - ((\sqrt{N}-1) \sin R) \cos \phi_{c,s}^{RIS} \cos \theta_{c,s}^{RIS})}]^T \quad (12)$$

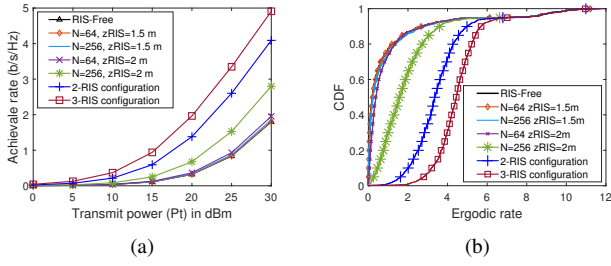


Fig. 2: (a) Ergodic rate vs transmit power; (b) empirical CDF.

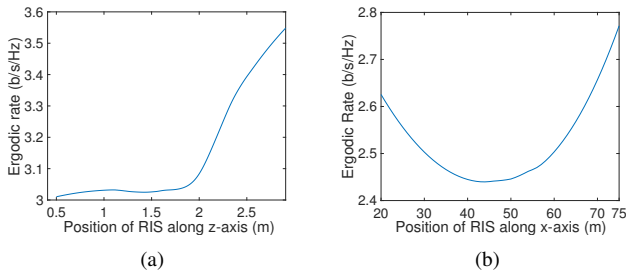


Fig. 3: Ergodic rate as a function of RIS positions: (a) Ergodic Rate as a function of the z position of RIS; (b) ergodic rate as a function of the x position of RIS.

A first simulation was conducted in Fig. 2 in order to showcase the comparison of RIS-assisted SREs through three configurations (single RIS, multiple RIS and RIS-free) and multiple parameters (the number of elements in each RIS surface and the position of RIS). An indoor environment is simulated here where the Tx, the Rx, the RIS in single-assisted channel, the second RIS in 2-RIS configuration and the third RIS in 3-RIS assisted environment are located at  $[0, 20, 2]$ ,  $[75, 35, 1]$ ,  $[75, 30, zRIS]$ ,  $[74, 30, 2]$ ,  $[71, 30, 2]$  respectively. We notice in Fig. 2(a) that RIS-free environment presents the lowest ergodic rate. The height of RIS is another crucial parameter for the ergodic rate. The number of elements present on a single RIS is a key element for the ergodic rate. It increases with the number of reflecting elements. Finally, the CDF in Fig. 2(b) as well as the the ergodic rate plots highlight the importance of the presence of multiple RIS in a radio environment for a better communication.

#### A. Optimal Placement of RISs

In this simulation, we explore optimal placement of RIS along the x-axis and z-axis. The Rx and Tx are located in their default location. In Fig. 3(a), the RIS is located at  $[75, 34, z]$  where z varies. Transmit power is fixed at 30dBm. As for the noise, it is set at -100dBm. The ergodic rate shows very small variations while z is between 0.5 and 2m. Once the RIS is higher than 2m, which is the level of the Tx, we

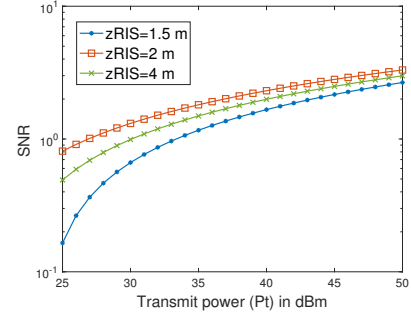


Fig. 4: Signal-to-noise ratio (SNR) in an RIS-assisted channel for different RIS height levels (zRIS).

notice a rapid increase in the rate. That is to say, placing the RIS above Tx constitutes an optimal placement since a LOS link is applied to the Tx-RIS channel by doing so.

In Fig. 3(b), the RIS is located at  $[x, 30, 2]$  for x varying from 20m to 75m where Tx and Rx are located respectively. Fig. 3(b) shows that the nearer the RIS gets either to the Rx or to the Tx, the rate rate increases. This is explained by the fact that the probability of the presence of a LOS link becomes higher in the RIS-Rx channel (when RIS is at the Rx side) or in the Tx-RIS channel (when RIS is at the Tx side), which means more significant received power. As a result, the ergodic rate increases considerably.

1) *Reliability Enhancement through RIS positioning*: While processing the (received) SNR for a simulated communication channel assisted by an RIS located in  $[75, 30, z]$  for different  $z \in (2, 3, 4)$  in Fig. 4, a considerable increase of SNR with the increase of the level of the RIS is noticeable. Also, for smaller values of transmit power, the gap in SNR between the sets of z-coordinates of RIS for different sets is wider. However, the value of the SNR gets higher for more powerful transmit power. In short, not only placing the RIS higher at or above the Tx antenna level increases the ergodic achievable rate, but it also enhances the reliability of the communication network.

#### B. Tilt and Rotation of RIS

We prove in this section that an RIS that focuses the reflected signal towards the Rx increases the ergodic rate. We apply 15 dBm transmit power and -100 dBm as noise power. Initially, the RIS is located at  $[70, 30, 2]$  at a  $0^\circ$  tilt angle on xz-plane. In Fig. 5(a), we plot the ergodic rate while we tilt the surface over x-axis to point towards the Rx which is located  $[70, 35, 1]$  (towards  $-80^\circ$ ). We repeat the same process in Fig. 5(b) with RIS located at  $[75, 35, 2]$  on yz-plane initially and rotating over y-axis to point towards the Rx.

Both of the simulations show an increase in the ergodic rate the moment we start tilting the RIS to point towards the Rx

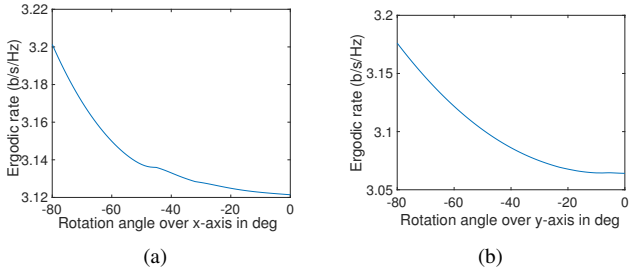


Fig. 5: (a) Ergodic rate as a function of RIS x-axis rotation where RIS in xz-plane initially; (b) ergodic rate as a function of RIS y-axis rotation where RIS in yz-plane initially.

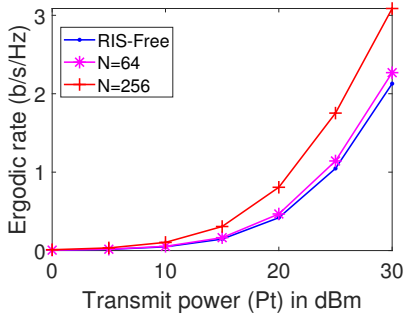


Fig. 6: Influence of number of elements ( $N$ ) on ergodic rate in a single-RIS configuration.

(in the order of 0.08 and 0.12 b/s/Hz for  $-80^\circ$  tilt angle). In short, this simulation proves that RIS performs better when it focuses the beam towards the Rx.

### C. Number of Reflecting Elements on an RIS

The reflecting elements on a single RIS allow the control of more impinging waves. At the Rx end, the received power is proportional to the square of the number of reflecting elements  $N$  which represents the number of the independently controlled phases from a single surface. The equation is as follows [14]:

$$P_r \approx (N + 1)^2 P_t \left( \frac{\lambda}{4\pi d} \right)^2, \quad (13)$$

where  $\lambda$  is the wavelength,  $d$  is the distance Tx-RIS-Rx and  $P_t$  is the transmit power. The following simulations show how both the capacity and reliability increase with  $N$ . Three plots corresponding to 3 values of  $N$  are shown in Fig. 6:  $N=64$  in purple, 256 in red and in blue, there is RIS-free environment. Two results can be deduced from it. First, the increasing capacity with the increasing  $N$  confirms what has been dictated in the theory. Second, the 64-element RIS does not bring major improvements to the environment.

### D. Optimal RIS Placement in a Multi-RIS Environment

We explore here the influence of multiple RIS configuration on the performance of the communication channel as a function of varying location of one RIS  $[x, 34, z]$  while fixing the location of the other one at  $[75, 30, 2]$ . In fig. 7(a),  $x$  varies between 25m and 75m and  $z$  fixed at 2m. In fig. 7(b),  $z$  varies between 1m and 3m. As a result, plots

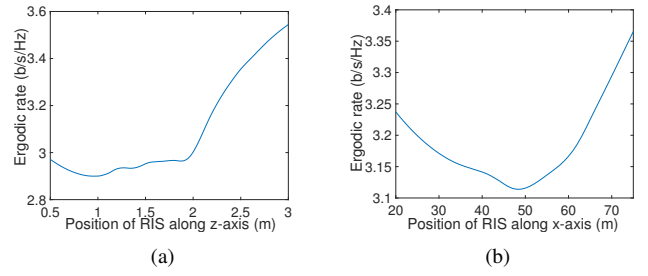


Fig. 7: Ergodic rate in a multiple RIS assisted environment: (a) Ergodic rate as a function of z-coordinates; (b) ergodic rate as a function of x-coordinates.

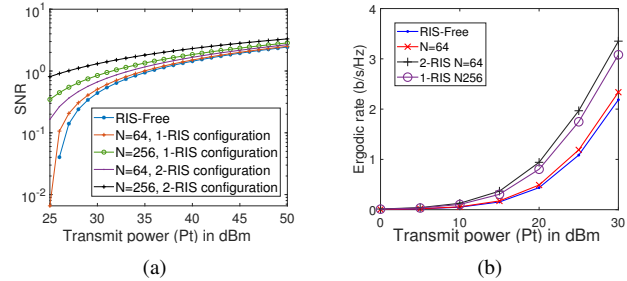


Fig. 8: Influence of number of elements ( $N$ ) in a multi-RIS configuration: (a) SNR; (b) ergodic rate.

held the same variation as the ones obtained in the previous section. Therefore, we conclude that ergodic rate increases when RIS gets closer to the base stations. Moreover, we achieve higher data rates when we implement RIS above the level of Tx ( $z=2$ m) because the probability of a LOS from Tx to the intelligent surface is higher. Furthermore, and most importantly, this simulation shows that we can achieve an additional 1 b/s/Hz gain in ergodic rate in a multiple-RIS configuration compared to single-RIS configuration.

### E. Impact of Number of Elements in a Multi-RIS Environment

The SNR simulation in Fig. 8(a) confirms the benefits of multiple RIS deployment and the increase of  $N$ . The reliability of the communication environment is enhanced with more RISs and a higher number of elements  $N$  on each surface. We notice a 0.4 dB SNR gain in 1-RIS configuration against 0.87 dB SNR gain in a multi-RIS configuration compared to RIS-free environment for a  $P_t = 26$  dBm. On the other hand, in the 64-element RIS case, it is no longer overlapping with RIS-free environment for multi-RIS configuration in Fig. 8(b). It also demonstrates similar performance as the 2-RIS configuration which increased the ergodic rate by 0.8 b/s/Hz for  $P_t = 30$  dBm. This highlights a trade-off consisting of whether to use a single RIS composed of 256 reflecting elements or 2-64 element RIS. It is a trade-off between deploying many RISs of smaller number of reflecting elements or deploying fewer RISs with higher number of elements.

### F. Multiple Users in an RIS-assisted Environment

RIS is envisioned within a communication platform that not only serves one but multiple users. In this section, we

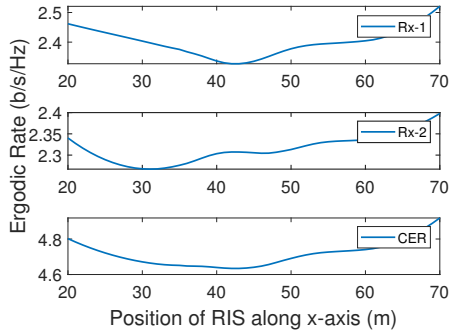


Fig. 9: Ergodic rate at user 1 and 2 (Rx-1, Rx-2) and cumulative ergodic rate (CER) in a 256-element RIS-assisted SRE where 128 elements are allocated for each user.

investigate the cumulative ergodic rate in a 2-user scenario through a single RIS assisted environment. The RIS consists of 256 controllable reflecting elements. In this simulation, we split those elements to serve the two users Rx-1 and Rx-2 positioned at [70, 32, 1] and [70, 35, 1] respectively. We allocate 128 reflecting elements of the RIS located at [x, 30, 2] for each user. We then plot in Fig. 9 the ergodic rate for each user as a function x that varying between 20 and 70. First thing to notice is that the closer the RIS gets to the users or the base station, the ergodic rate increases. On the other hand, the two users are two metres apart in the y-axis, which slightly impacts capacity performance with a 0.125 b/s/Hz difference between the users. Nevertheless, the ergodic rate is much higher for both users by allocating a certain number of elements to the users by only using a single RIS compared to the ergodic rate in RIS-free environment present in Fig. 2(a) where for 30 dBm transmit power, the ergodic rate is less than 2 b/s/Hz. This opens up the door towards future research opportunities that covers an optimal reflecting elements' allocation that could maintain steady and even performance for the users.

## V. KEY INSIGHTS AND CONCLUDING REMARKS

RIS is a promising technology for 6G wireless systems. It was the aim of this paper to conduct a holistic evaluation of RIS-assisted SREs. We have conducted a simulation-drive performance evaluation under different scenarios and configurations. The key findings and insights on system performance are highlighted as follows.

- Optimal RIS placement is next to the endpoints (Tx or Rx) and above Tx level where the capacity increases by 0.3 b/s/Hz near the Rx and by 0.2 b/s/Hz by the Tx. SNR also increases from 0.165 dB in case for 1.5m RIS elevation from the ground to 0.810 dB for 4m elevation, scoring a gain of 0.645 dB. Moreover, the ergodic rate in an RIS- assisted SRE increases with the number of reflecting elements present on a single RIS. It increased from 2.1 b/s/Hz in an RIS-free environment to 2.3 b/s/Hz for 64-element and 3.1 b/s/Hz for 256-element RISs.
- Multiple RIS-assisted smart radio environment drastically improves capacity and reliability. It has shown an increase

of 1 b/s/Hz in ergodic rate and 0.46 dB in SNR for a 256 element 2-RIS configuration compared to a single-RIS environment for 25 dBm transmit power. This multiple RIS configuration has also proven its effectiveness for a 64-element RIS. As a matter of fact, ergodic rate augmented from 2.3 b/s/Hz in a single 64-element RIS (a slightly improved communication environment) to 3.3 b/s/Hz in a 2-RIS configuration (a stronger performance similar to single 256-element RIS configuration).

- The tilt (rotations over x-axis and y-axis) of the RIS was also investigated. We found that directing the beam to point to the receiver by tilting the RIS increased the capacity by 0.11 b/s/Hz.
- In the case of multiple users in a 256-element RIS assisted environment, we split the reflecting elements from the RIS to serve both users by allocating 128 elements for each. We noticed a better performance with an increased ergodic rate for both users with a slight 0.12 b/s/Hz difference between the two.

Key future work directions include optimal design of an SRE with a single RIS having sufficiently large number of elements or multiple RISs with relatively small number of elements and adaptive allocation of elements to each receiver in multi-user environments.

## REFERENCES

- [1] M. Di Renzo *et al.*, "Smart Radio Environments Empowered by Reconfigurable Intelligent Surfaces: How it Works, State of Research, and Road Ahead," *IEEE J. Sel. Areas Commun.*, pp. 1–1, 2020.
- [2] D. Kudathanthirige, D. Gunasinghe, and G. Amarasinghe, "Performance Analysis Of Intelligent Reflective Surfaces For Wireless Communication," *arXiv preprint arXiv:2002.05603*, 2020.
- [3] S. Hu and F. Rusek, "Spherical Large Intelligent Surfaces," in *IEEE ICASSP*, 2020, pp. 8673–8677.
- [4] K. Ntontin *et al.*, "Reconfigurable Intelligent Surfaces vs. Relaying: Differences, Similarities, And Performance Comparison," *arXiv preprint arXiv:1908.08747*, 2019.
- [5] E. Björnson, Ö. Özdogan, and E. G. Larsson, "Intelligent Reflecting Surface versus Decode-and-forward: How Large Surfaces Are Needed to Beat Relaying?" *IEEE Wireless Commun. Lett.*, vol. 9, no. 2, pp. 244–248, 2019.
- [6] A. A. Boulogeorgos and A. Alexiou, "performance analysis of reconfigurable intelligent surface-assisted wireless systems and comparison with relaying," *IEEE Access*.
- [7] D. Dardari, "Communicating With Large Intelligent Surfaces: Fundamental Limits And Models," *IEEE J. Sel. Areas Commun.*, 2020.
- [8] E. Björnson and L. Sanguinetti, "Power Scaling Laws and Near-Field Behaviors of Massive MIMO and Intelligent Reflecting Surfaces," *arXiv preprint arXiv:2002.04960*, 2020.
- [9] J. He *et al.*, "Large Intelligent Surface for Positioning in Millimeter Wave MIMO Systems," in *IEEE VTC*, 2020, pp. 1–5.
- [10] —, "Adaptive Beamforming Design for Mmwave RIS-aided Joint Localization and Communication," in *IEEE WCNC Workshops*, 2020, pp. 1–6.
- [11] E. Basar *et al.*, "Indoor and Outdoor Physical Channel Modeling and Efficient Positioning For Reconfigurable Intelligent Surfaces in MmWave Bands," *arXiv preprint arXiv:2006.02240*, 2020.
- [12] I. Yildirim, E. Basar, and I. Akyildiz, "Modeling and Analysis of Reconfigurable Intelligent Surfaces for Indoor and Outdoor Applications in 6G Wireless Systems," 2020.
- [13] H. K *et al.*, "5G 3GPP-Like Channel Models for Outdoor Urban Microcellular and Macrocellular Environments," in *2016 IEEE 83rd Vehicular Technology Conference (VTC Spring)*, 2016, pp. 1–7.
- [14] E. Basar, I. Yildirim, and I. F. Akyildiz, "Wireless Communications Through Reconfigurable Intelligent Surfaces," *IEEE Access*, vol. 7, pp. 116753–116773, 2019.